DFT-Based Spectral Precoding for Scalable Unique-Word OFDM

Salil Sharma*†, *Member, IEEE*, Syed Waqas Haider Shah*‡, *Member, IEEE*, Jesus O. Lacruz*, *Member, IEEE* and Joerg Widmer*, *Fellow, IEEE*
*IMDEA Networks Institute, Spain, † Universidad Carlos III de Madrid, Spain, ‡ University of Cambridge, UK
{salil.sharma, syed.waqas, jesusomar.lacruz, joerg.widmer}@networks.imdea.org, sw920@cam.ac.uk

***Abstract*—Unique-word orthogonal frequency division multiplexing (UW-OFDM) addresses the spectral inefficiency of cyclic prefix (CP) OFDM by embedding the guard interval within the symbol period. However, its practical adoption is hindered by a prohibitive computational bottleneck. Conventional methods for embedding unique word within the DFT window rely on complex matrix inversions at the transmitter (Tx). While alternative zero-padded (ZP) schemes avoid this complexity, they place guard interval outside DFT window, breaking natural circularity and necessitating noise-enhancing Overlap-Add receiver (Rx). This letter proposes a scalable, closed-form isometric Spectral Precoding architecture that resolves this trade-off. By exploiting frequency-domain interpolation, we implicitly construct the required near-zero-energy tail within the DFT window using only deterministic linear transformations. We prove this construction reduces Tx complexity to log-linear order while preserving standard single-tap equalization without Rx noise enhancement. Validated with 5G-NR numerologies, the scheme matches CP-OFDM error performance while eliminating CP overhead.**

***Index Terms*—Orthogonal Frequency Division Multiplexing (OFDM), 5G-NR, 6G, Unique-word OFDM, Cyclic Prefix (CP)**

I. Introduction

Multi-carrier modulation schemes, especially orthogonal frequency division multiplexing (OFDM), play a pivotal role in modern wireless communications. The effectiveness of OFDM in mitigating frequency-selective channels has led to its widespread adoption across contemporary wireless networks [1, 2]. Recent comprehensive surveys indicate that this dominance will extend into the sixth-generation (6G) era, where OFDM is projected to serve as the underlying physical layer framework even as new modulation schemes are introduced [3, 4]. Despite its success, traditional OFDM relies on a guard interval to mitigate inter-symbol interference (ISI). The most common variant, cyclic-prefix OFDM (CP-OFDM), as shown in Fig. 1, appends a copy of the signal tail to the beginning of the symbol. This simplifies Rx design by transforming linear convolution into circular convolution, facilitating single-tap equalization. However, the CP represents a significant spectral inefficiency, as it consumes time resources with redundant symbols that do not convey useful information.

To address this, deterministic guard interval schemes have been proposed, but they historically force a trade-off between Tx and Rx complexity. A common alternative is zero-padded (ZP) OFDM or known-sequence (KS) OFDM [5]. These methods append a guard interval outside the DFT window. While computationally cheap to transmit, this external padding does not form a circular convolution with the channel. Consequently, the Rx must employ overlap-and-add (OLA) processing which degrades signal-to-interference-plus-noise ratio (SINR) by folding tail noise back into the symbol or complex iterative equalizers to restore orthogonality [5]. This increased Rx complexity and noise penalty prevents ZP-OFDM from replacing CP-OFDM in standard-compliant systems.

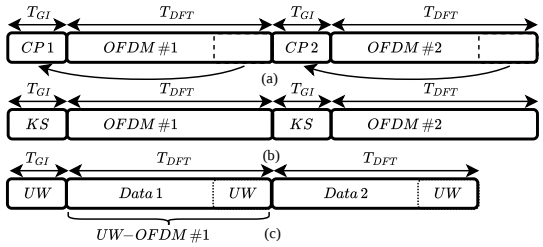

Fig. 1: Time-domain transmit data structures for (a) CP-OFDM, (b) KS-OFDM and (c) UW-OFDM.

Unique-word OFDM (UW-OFDM) resolves this by embedding the deterministic sequence within the effective DFT interval (typically at the tail) [6–8]. Because the tail is an intrinsic part of the core OFDM symbol, it acts as a natural cyclic extension for the subsequent symbol. This preserves the simple single-tap frequency domain equalization (FDE) of CP-OFDM without the noise enhancement of OLA Rxs. Furthermore, the presence of deterministic UWs enables secondary applications such as synchronization and channel estimation [9, 10]. Recent works have further demonstrated the versatility of UW-OFDM, extending its application to space-time block coding (STBC) [11], and bistatic integrated sensing and communication (ISAC) systems [12], while maintaining superior error-rate performance over CP-OFDM [13, 14].

Despite these advantages, practical UW-OFDM implementation faces a critical computational bottleneck at the Tx. Existing schemes are generally categorized as systematic and non-systematic. In systematic designs, redundant subcarriers are utilized to force a near-zero-energy guard tail [15]. However, these designs suffer from excessive power overhead on the redundant carriers (often exceeding 30 dB), which is infeasible for practical systems [16]. Conversely, non-systematic designs distribute redundancy across the entire spectrum, offering superior power efficiency [8, 13]. However, these typically require complex generator matrices derived via iterative solvers or matrix inversions, making them computationally intensive

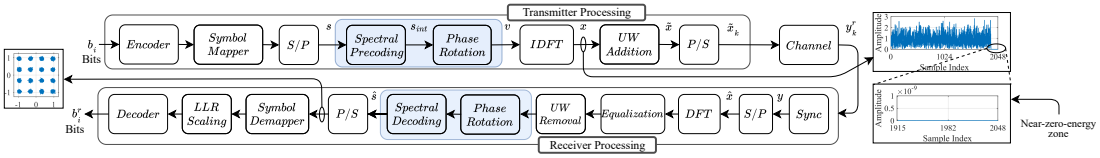

Fig. 2: Baseband Tx/Rx model of the proposed UW-OFDM system. Spectral Precoding expands N_d logical subcarriers to N physical ones (expansion factor $\alpha = N/N_d$), followed by phase rotation. This creates a time-domain near-zero-energy zone of length $N_r = (\alpha - 1)N_d$ at the symbol tail. (Configuration: 5G-NR numerology with $N = 2048$ and $N_d = 1914$, see Table II.)

and ill-suited for large-subcarrier systems.

To bridge this gap, this letter proposes a low-complexity, non-systematic UW-OFDM framework utilizing optimization-free sequence construction. Specifically, we introduce a DFT-based spectral precoder that employs frequency-domain interpolation to map data symbols onto an expanded set of physical subcarriers. This interpolated sequence then undergoes a deterministic phase rotation to implicitly construct a near-zero-energy guard interval at the symbol tail, entirely avoiding computationally expensive iterative solvers or matrix inversions. Analytically, we demonstrate via matrix formulation that this closed-form design accommodates arbitrary subcarrier configurations while maintaining the log-linear computational complexity order of standard OFDM. Finally, the framework's scalability and adaptability are validated via Monte Carlo simulations using 3GPP-defined 5G-NR numerologies, confirming Bit Error Rate (BER) parity with conventional CP-OFDM.

II. UW-OFDM: A Primer

We consider an N-subcarrier UW-OFDM system where N_d subcarriers carry data and the remaining $N_r = (N - N_d)$ subcarriers carry redundancy [7]. Let $\boldsymbol{s} \in \mathbb{C}^{N_d}$ denote the vector of information symbols, where the entries of $\boldsymbol{s}$ are drawn from a quadrature amplitude modulation (QAM) constellation. In a general framework, $\boldsymbol{s}$ is linearly transformed by a code generator matrix $\boldsymbol{G} \in \mathbb{C}^{N \times N_d}$ and mapped to physical resource channels via a mapping matrix $\boldsymbol{B} \in \{0,1\}^{N \times N}$. The resulting frequency-domain sequence undergoes an inverse DFT (IDFT) operation, producing a time-domain waveform explicitly constructed to possess a near-zero-energy interval at the tail. This relationship can be expressed in matrix form as

$$\boldsymbol{x} = [\boldsymbol{x}_d^T, \boldsymbol{0}_{N_r}^T]^T = \boldsymbol{F}_N^H \boldsymbol{B}\boldsymbol{G}\boldsymbol{s}, \tag{1}$$

where $\boldsymbol{x}$ represents the time-domain UW-OFDM symbol (prior to UW insertion), consisting of the data portion $\boldsymbol{x}_d$ of length N_d and a near-zero-energy guard interval $\boldsymbol{0}_{N_r}$ of length N_r. Here, $\boldsymbol{F_N}$ represents the N-point unitary DFT matrix and $(\cdot)^H$ is the Hermitian transpose. Subsequently, the deterministic UW $\boldsymbol{x}_{uw}$ is added to the guard interval, yielding the final transmit symbol $\tilde{\boldsymbol{x}} = [\boldsymbol{x}_d^T, \boldsymbol{x}_{uw}^T]^T$. Hence, the primary design objective is to construct $\boldsymbol{G}$ such that the null-space constraint in (1) is strictly satisfied, ensuring interference-free insertion of UW. Broadly, construction of $\boldsymbol{G}$ falls into two paradigms, each presenting distinct trade-offs, as given in the following.

1) Systematic Designs: In this, generator matrix is designed as $\boldsymbol{G} = [\boldsymbol{I}_{N_d}^T, \boldsymbol{G}_r^T]^T$, where $\boldsymbol{G_r}$ is the redundancy submatrix of the transformation matrix. While the identity component $\boldsymbol{I}_{N_d}$ preserves the original data symbols and simplifies Rx processing, it forces the redundant subcarriers to absorb the entire cancellation energy. This results in severe power spikes, with overhead often exceeding 30 dB in large systems [15, 16]. Consequently, systematic designs face a critical challenge of excess power, reducing Tx's overall energy efficiency.

2) Non-Systematic Designs: These designs distribute redundant information throughout the spectrum, allowing better power uniformity and frequency diversity [13]. However, deriving such matrices typically requires solving complex numerical optimization problems to satisfy the constraint in (1). Although optimization yields spectral benefits, computational complexity scales poorly with N, making them prohibitive for modern high-bandwidth standards like 5G and beyond [17].

III. Proposed UW-OFDM Design

We propose a low-complexity, non-systematic UW-OFDM framework designed explicitly for scalability in large-subcarrier systems. Unlike preceding methods that rely on complex numerical optimization to obtain the generator matrix, our approach employs a deterministic, closed-form design that significantly reduces implementation complexity. The transceiver architecture is shown in Fig. 2 [1]. The input binary stream, b_i, is encoded and QAM-modulated to form data symbol vector $\boldsymbol{s} \in \mathbb{C}^{N_d}$, corresponding to N_d orthogonal logical channels. Subsequently, spectral precoding block generates the interpolated vector $\boldsymbol{s}_{\text{int}} \in \mathbb{C}^N$, which represents spectrally interpolated version of $\boldsymbol{s}$ with an expansion factor of $\alpha = \frac{N}{N_d}$.

This spectral interpolation strategy, which effectively utilizes frequency-domain zero-padding to expand the signal dimension, is designed to implicitly generate a near-zero-energy zone in the time domain. Unlike rigid code-based designs, this approach is inherently flexible for arbitrary (N_d, N_r) configurations. Subsequently, the Phase-Rotation block applies a deterministic phase shift to each element of the interpolated vector $\boldsymbol{s}_{\text{int}}$. Specifically, the k-th subcarrier is rotated by a factor of $e^{-j\frac{2\pi kl}{N}}$, where l denotes the required cyclic shift in time-domain samples. This linear phase transformation results in a cyclic shift of the time-domain signal, aligning the implicit null-zone with the symbol tail. The resulting precoded vector, denoted as $\tilde{\boldsymbol{s}}$, is transformed to the time domain using a N-point IDFT. Finally, the UW Addition block superimposes a

[1]The proposed design strictly complies with 3GPP 5G-NR specifications for high-numerology operation, using a subcarrier spacing (SCS) of 240 kHz, $N = 2048$ physical subcarriers and $N_d = 1914$ logical subcarriers. It reflects the standard configuration defined for FR2 operation and ensures consistency with standardized CP-OFDM processing. See Section IV and Table II.

deterministic UW sequence onto the last N_r samples of the time-domain signal, filling the reserved guard interval.

A. Tx Processing: Spectral Precoding & Phase Rotation

The core novelty of the proposed scheme lies in the DFT-based generation of the near-zero-energy zone. Exploiting the well-established principle of zero-padded signal interpolation [18], the proposed *Spectral Precoder* performs frequency-domain interpolation to map $\boldsymbol{s}$ onto the N physical subcarriers. This is mathematically realized by a cascade of a forward DFT, zero-padding, and an inverse DFT, as shown in Fig. 3. We define the precoding operation as

$$\boldsymbol{v} = \boldsymbol{\Phi}^{l} \underbrace{(\boldsymbol{F}_N^H \boldsymbol{Z} \boldsymbol{F}_{N_d})}_{\text{Interpolation}} \boldsymbol{s} \tag{2}$$

where $\boldsymbol{F}_{N_d}$ and $\boldsymbol{F}_N$ are unitary DFT matrices of size N_d and N, respectively. Matrix $\mathbf{Z} \in \mathbb{R}^{N \times N_d}$ is a zero-padding matrix that inserts N_r zeros at the center of the DFT band to perform ideal low-pass interpolation, as shown in Fig. 3. The interpolated vector is then phase-rotated using the diagonal matrix $\boldsymbol{\Phi}^l = \mathrm{diag}(1, e^{-j\frac{2\pi l}{N}}, \ldots, e^{-j\frac{2\pi l(N-1)}{N}})$, which produces a circular time-domain shift of l samples. To align the implicit near-zero-energy zone with the symbol tail [2] (samples $N_d{+}1$ to N), we set $l = -(N_d/2{-}1)$. Final time-domain transmit signal, after adding $\mathbf{x}_{uw}$ becomes $\tilde{\boldsymbol{x}} = \boldsymbol{F}_N^H \boldsymbol{v} + [\mathbf{0}_{N_d}^T, \boldsymbol{x}_{uw}^T]^T$. This construction ensures that the tail-region energy is negligible prior to UW insertion, thereby minimizing interference.

B. Rx Processing

At Rx, the scheme preserves standard OFDM processing. The deterministic UW serves as a guard interval longer than the channel delay spread, ensuring circular convolution for efficient single-tap FDE. Consequently, the receiver extracts exactly N samples for direct FFT processing, inherently preserving circularity without the noise-enhancing OLA stage required by ZP-OFDM [5]. After synchronization, the received signal is FFT-processed and equalized using standard FDE. Because the UW is deterministic, its frequency response is known and can be directly subtracted from the equalized symbols, eliminating its contribution without additional estimation. The estimated data symbols $\hat{\mathbf{s}}$ are then recovered by reversing the spectral precoding operations.

$$\hat{\boldsymbol{s}} = (\boldsymbol{F}_{N_d}^H \boldsymbol{Z}^T \boldsymbol{F}_N \boldsymbol{\Phi}^{-l})(\boldsymbol{H}_{eq} \boldsymbol{F}_N \boldsymbol{y} - \boldsymbol{F}_N [\mathbf{0}_{N_d}^T, \boldsymbol{x}_{uw}^T]^T) \tag{3}$$

Here, $\mathbf{H}_{eq}$ denotes the channel equalization matrix. The operation $\mathbf{Z}^T$ performs decimation by discarding the zero-padded samples in the virtual time domain, thereby recovering the original N_d-point logical sequence. This linear recovery preserves the low-complexity advantage of the proposed framework. The estimated symbol vector $\hat{\mathbf{s}}$ is then demapped to compute log-likelihood ratios (LLRs) for forward error correction. These LLRs are weighted by the effective gains of the logical channels; hence, the estimated per-subcarrier CSI undergoes the same spectral projection as $\hat{\mathbf{s}}$ in (3), mapping the physical subcarrier responses onto the N_d logical channels prior to LLR weighting ($\boldsymbol{LLR}_{weights} = |(\boldsymbol{F}_{N_d}^H \boldsymbol{Z}^T \boldsymbol{F}_N \boldsymbol{\Phi}^{-l}) \boldsymbol{H}_{eq}|$).

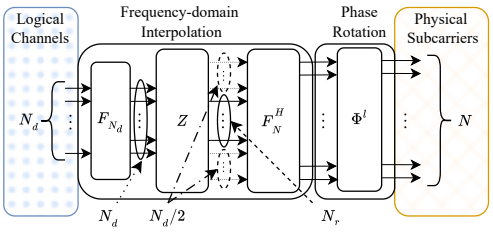

Fig. 3: Schema of frequency-domain interpolation and phase rotation process, showing the mapping of N_d logical channels to N physical subcarriers through mid-band zero insertion.

Remark: (Conservation Properties): Unlike systematic designs that suffer from significant power penalties, the proposed transceiver is strictly energy-conserving. By inspecting the precoder structure in (2), we observe that $\boldsymbol{F}$ and $\boldsymbol{\Phi}$ are unitary matrices, and $\boldsymbol{Z}$ is a semi-unitary isometric mapping ($\boldsymbol{Z}^T\boldsymbol{Z} = \boldsymbol{I}_{N_d}$). Consequently, the mean transmit energy is $E[|\tilde{\boldsymbol{x}}|^2] = E[|\boldsymbol{s}|^2] \cdot \mathrm{tr}(\boldsymbol{Z}^T\boldsymbol{Z}) = N_d\sigma_s^2$. This confirms there is no power overhead. Furthermore, this semi-unitary structure implies that the transformation is isometric, thereby preserving the Euclidean distance between any two transmit vectors relative to the input constellation. For any distinct pair of input symbol vectors $(\boldsymbol{s}_i, \boldsymbol{s}_j)$, the Euclidean distance is strictly preserved as $|\tilde{\boldsymbol{x}}_i - \tilde{\boldsymbol{x}}_j|^2 = |\boldsymbol{s}_i - \boldsymbol{s}_j|^2$. This guarantees that the minimum distance (d_{min}) remains the same, ensuring that no BER degradation occurs relative to standard OFDM.

C. Computational Complexity Analysis

We analyze the computational complexity of the proposed UW-OFDM Tx. The transmit signal is given by: $\boldsymbol{x} = \boldsymbol{F}_N^H \boldsymbol{\Phi}^l (\boldsymbol{F}_N^H \boldsymbol{Z} \boldsymbol{F}_{N_d}) \boldsymbol{s}$. In a direct matrix implementation, spectral interpolation and phase rotation are performed via successive matrix-vector multiplications, requiring $(2N^2 + N_d^2 + N)$ complex-multiplications [19]. This form is primarily theoretical; practical implementations exploit the structure of the involved operators. In contrast, prior systematic and non-systematic UW-OFDM schemes incur a real-time complexity dominated by a matrix-vector multiplication $\boldsymbol{Gs}$, yielding

TABLE I: Complexity Comparison of UW-OFDM Designs

Transmission Scheme	Operation	Approx. Real FLOPS	Asymptotic Order
Standard CP-OFDM	$\boldsymbol{F}_N^H \boldsymbol{Bs}$	$5N\log_2 N$	$\mathcal{O}(N\log_2 N)$
UW-OFDM (Sys./Non-Sys.)	$\boldsymbol{F}_N^H \boldsymbol{BGs}$	$8NN_d - 2N$ $+5N\log_2 N$	$\mathcal{O}(NN_d)$
Proposed Method (Standard)	$\boldsymbol{F}_N^H \boldsymbol{\Phi}^l \boldsymbol{F}_N^H \boldsymbol{Z} \boldsymbol{F}_{N_d} \boldsymbol{s}$	$\sim 5N_d\log_2 N_d$ $+10N\log_2 N + 6N$	$\mathcal{O}(N\log_2 N)$
Proposed Method (Fast)	$\boldsymbol{S}^l \boldsymbol{J} \boldsymbol{Z} \boldsymbol{F}_{N_d} \boldsymbol{s}$	$\sim 5N_d\log_2 N_d$	$\mathcal{O}(N_d\log_2 N_d)$

[2]To quantitatively characterize this guard interval, we define the discrete-time Signal-to-Leakage Ratio (SLR) for the precoded sequence $\boldsymbol{x} = \boldsymbol{F}_N^H \boldsymbol{v}$ prior to UW insertion as SLR (dB) = $10\log_{10}(P_{data}/P_{tail})$, where P_{data} and P_{tail} are the average powers of the data and tail samples, respectively. For the implementation as per (2), finite-precision floating-point arithmetic generates infinitesimal computational limits (e.g., amplitude errors $\sim 10^{-9}$), yielding a simulated SLR bounded only by machine precision (> 150 dB). Furthermore, in the practical fast implementation (Section III-C), this tail is generated via explicit digital memory-padding, rendering the discrete tail samples mathematically exact zeros (SLR $\to \infty$). Thus, within the discrete baseband scope, the interval acts as a perfect guard zone.

TABLE II: Simulation Parameters

Parameter	CP-OFDM	Proposed UW-OFDM
Modulation Scheme	4-QAM, 16-QAM, 64-QAM	
Total Subcarriers (N)	2048	
Data Carriers (N_d)	2048	1914
Redundant Carriers (N_r)	0	134
Guard/UW Length	N_{cp} = 144	N_{uw} = 134
Total Symbol Duration	2192 samples	2048 samples
Spectral Efficiency	$N_d/(N+N_{cp}) \approx 93.4\%$	$N_d/N \approx 93.4\%$
Channel Model	AWGN, Extended Vehicular A (EVA)	
Coding	LDPC (Interleaved), Rate = 3/4	

$\mathcal{O}(NN_d)$ complexity [19]. While recent literature has proposed advanced matrix optimization methods and data-driven approaches to manage this operational cost [20, 21], such schemes remain fundamentally bottle-necked by matrix-vector multiplication structures at the transmitter, unlike pure FFT-based architectures. Since $N_d \approx N$, this is substantially higher than the $\mathcal{O}(N \log_2 N)$ complexity of conventional CP-OFDM. Detailed computational complexity, measured in real floating-point operations (FLOPs) per [19], is given in Table I.

The proposed design significantly reduces complexity by using DFT properties. After regrouping linear operators

$$\boldsymbol{x} = (\boldsymbol{F}_N^H \boldsymbol{\Phi}^l \boldsymbol{F}_N)(\boldsymbol{F}_N^H \boldsymbol{F}_N^H)\boldsymbol{Z}\boldsymbol{F}_{N_d}\boldsymbol{s} = \boldsymbol{S}^l \boldsymbol{J}\boldsymbol{Z}(\boldsymbol{F}_{N_d}\boldsymbol{s}), \quad (4)$$

where $\boldsymbol{S}^l = \boldsymbol{F}_N^H \boldsymbol{\Phi}^l \boldsymbol{F}_N$ is a time-domain circular shift matrix with lag l, while $\boldsymbol{J} = \boldsymbol{F}_N^H \boldsymbol{F}_N^H$ is a permutation (flip) matrix.

This derivation shows that the proposed Tx does not require three DFT/IDFT operations, but only a single N_d-point DFT ($\boldsymbol{F}_{N_d}\boldsymbol{s}$). Essentially, this reveals a powerful duality; we achieve the spectral shaping of an N-subcarrier UW-OFDM system using only the computational footprint of an N_d-point transform. Since standard 5G-NR subcarrier allocations (N_d) are composite numbers with small prime factors (2, 3, and 5), this transform is efficiently implemented using mixed-radix FFTs, preserving $\mathcal{O}(N_d \log_2 N_d)$ complexity. The remaining operations zero-padding ($\boldsymbol{Z}$), flipping ($\boldsymbol{J}$), and circular shifting ($\boldsymbol{S}^l$) are low-complexity memory operations. Consequently, the overall complexity is dominated by $\mathcal{O}(N_d \log_2 N_d)$, which is lower than the $\mathcal{O}(N \log_2 N)$ complexity of conventional CP-OFDM. Although a forward DFT is required, compatibility with standard OFDM hardware is maintained, as the DFT can be implemented using a conventional IFFT via index reversal.

IV. Evaluation and Discussion

Now we evaluate link-level and physical-layer performance of the proposed framework. Simulation parameters (Table II) follow 3GPP 5G-NR specifications for high-numerology operation (SCS = 240 kHz). To ensure a fair comparison, the UW-OFDM subcarrier allocation (N_d = 1914, N_r = 134) is selected to match the spectral efficiency of the reference CP-OFDM system. The Tx employs a phase-rotation parameter $l = -(N_d/2 - 1) = -956$ to align the near-zero-energy region with the symbol tail. Interleaved LDPC coding with rate $R = 3/4$ is used [1, 2]. The channel follows the 3GPP EVA model to capture frequency-selective fading. At Rx, perfect synchronization is assumed, UW samples are removed before FFT, and MMSE FDE is applied with perfect CSI. Results are averaged over 5,000 independent channel realizations.

We further assess physical signal properties to verify that spectral precoding introduces no power penalty or spectral regrowth. Energy conservation is evaluated via the complementary cumulative distribution function (CCDF) of total symbol power and peak-to-mean envelope power ratio (PMEPR) using 10^6 independent symbol realizations. Results are compared for CP-OFDM, UW-OFDM with a zero-padded guard, and UW-OFDM with a deterministic polyphase UW. Spectral containment is analyzed through the averaged PSD computed over 1,000 symbols using a rectangular-window periodogram. For fair mask comparison, CP-OFDM employs 308 null subcarriers, while UW-OFDM uses 288 null logical channels, which map (via the spectral expansion factor $2048/1914$) to an equivalent physical guard band of approx. 308 subcarriers.

A. Physical Layer Characterization

We first assess the physical signal properties to verify that the proposed spectral precoding preserves the fundamental energy and statistical characteristics of the OFDM waveform. *1) Power Conservation:* Fig. 4a shows the CCDF over 10^6 i.i.d. symbol realizations. For the proposed UW-OFDM with a zero-padded guard ($\mathbf{x}_{uw} = \mathbf{0}$), the statistical distribution profile perfectly mirrors the trend of CP-OFDM, confirming that the precoder in (2) is a semi-unitary isometric operator and introduces no power overhead. However, because its active energy originates from only N_d logical channels, its absolute total symbol power is proportionately lower. When a deterministic polyphase UW (e.g., Zadoff-Chu) is added, the power distribution shifts to perfectly overlap with the CP-OFDM baseline, indicating that any increase is purely additive and due solely to the UW energy, and not precoding structure. *2) PMEPR:* Fig. 4c evaluates the amplitude statistics of the transmitted signal. Despite concerns of peak regrowth typically associated with interpolation-based schemes, the proposed waveform exhibits a PMEPR distribution that almost coincides with CP-OFDM. This confirms that the peak behavior remains dominated by the IFFT operation rather than the spectral precoding. Furthermore, populating the time-domain near-zero-energy zone with a constant-envelope polyphase UW elegantly restores the mean symbol power without introducing new amplitude peaks. Consequently, the overall PMEPR strictly aligns with that of CP-OFDM, ensuring seamless compatibility with existing power-amplifier back-off requirements.
3) Spectral Containment: Finally, Fig. 4e shows that the average PSD of UW-OFDM closely matches that of CP-OFDM, with identical roll-off characteristics. This verifies that the implicit time-domain windowing induced by interpolation creates the desired near-zero-energy zone without spectral regrowth or out-of-band leakage.

B. Link-Level Performance

Link-level reliability is evaluated in terms of BER. First, we establish a performance baseline in the AWGN channel as shown in Fig. 4b (uncoded) and Fig. 4d (LDPC coded). The proposed UW-OFDM achieves identical BER performance to CP-OFDM across all modulation orders, confirming that the DFT-based precoder and phase rotation preserve Euclidean

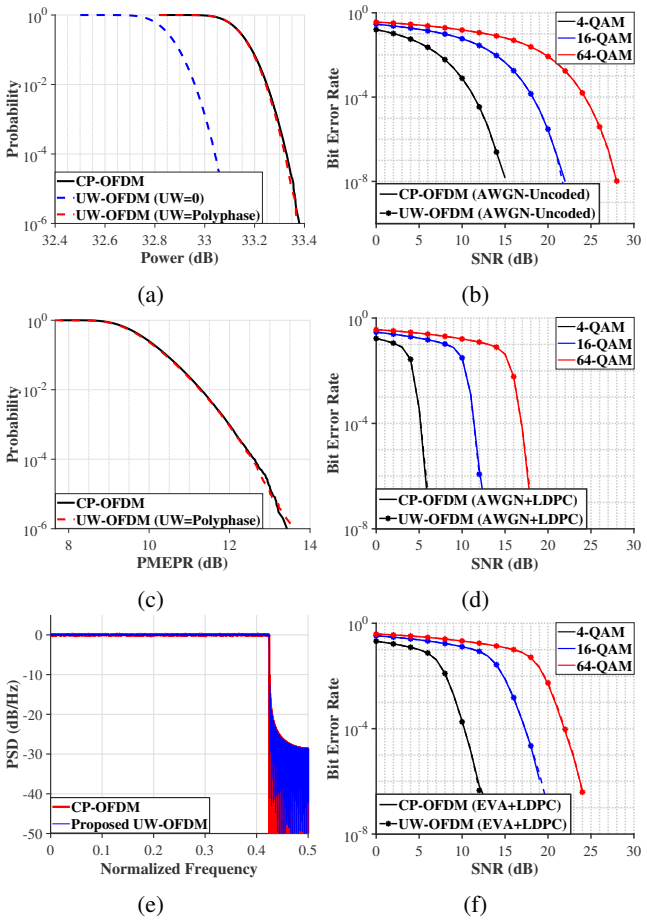

Fig. 4: Performance comparison of the proposed UW-OFDM framework and CP-OFDM: (a) Total-symbol-power CCDF, (b) Uncoded BER in AWGN, (c) PMEPR CCDF, (d) BER in AWGN with LDPC (3/4 coding rate), (e) PSD comparison, and (f) BER in EVA multipath with LDPC (3/4 coding rate).

distance between constellation points, thereby causing no performance degradation in AWGN channels.

Next, we evaluate robustness against frequency-selective fading using the 3GPP EVA channel model. As shown in Fig. 4f, the proposed scheme effectively suppresses ISI without a conventional CP. The circular phase rotation preserves the circular convolution property, enabling standard single-tap FDE. Consequently, the BER performance matches that of CP-OFDM, achieving full diversity without an error floor. At higher SNRs, the proposed scheme maintains a marginal performance advantage. This confirms that the implicitly generated near-zero-energy guard interval provides sufficient isolation against multipath delay spread (where $N_{uw} > \tau_{max}$), validating it as a low-complexity alternative.

V. Conclusion

This letter establishes that low-complexity UW-OFDM transmission is achievable without the penalties of complex iterative optimization or excessive power overhead. By introducing a closed-form DFT-based spectral precoder, we successfully exploit the duality between frequency-domain interpolation and time-domain energy confinement to construct a deterministic guard interval. Crucially, the analytical derivation proves that the Tx complexity scales with $\mathcal{O}(N_d \log_2 N_d)$, breaking the computational bottleneck that has historically hindered the adoption of non-systematic UW-OFDM in large-subcarrier systems. Validated against 3GPP 5G-NR standards, the proposed framework maintains BER performance equivalent to conventional CP-OFDM while offering the spectral advantages of a near-zero-energy tail. This combination of logarithmic complexity and strict standards compliance positions the design as a robust, scalable candidate for next-generation high-bandwidth waveforms, particularly where latency and processing power are constrained.

VI. Acknowledgment

This work is funded by the European Union (EU) grant agreement 101192521 (MultiX) and 101129618 (UNITE), and TUCAN6-CM (TEC-2024/COM-460) and DISCO6G-CM (TEC-2024/COM-360) funded by the Comunidad de Madrid (ORDEN 5696/2024). The work of Syed Waqas Haider Shah was supported by MSCA-PF project 6G-SCOUT under grant 101199056 funded by EU Horizon Europe Programme.

References

[1] "IEEE std 802.11-2024, part 11: Wireless LAN medium access control (MAC) and physical layer (PHY) specifications," *IEEE Std 802.11-2024 (Revision of IEEE Std 802.11-2020)*, pp. 1–5956, 2025.

[2] 3GPP, "NR; Physical channels and modulation," *Technical Specification Group TSG SA, Tech. Rep. 38.211 (Version 18.2.0)*, 2024.

[3] M. S. J. Solaija, S. E. Zegrar, and H. Arslan, "Orthogonal frequency division multiplexing: The way forward for 6G physical layer design?" *IEEE Veh. Technol. Mag.*, vol. 19, no. 1, pp. 45–54, 2024.

[4] J. G. Andrews, T. E. Humphreys, and T. Ji, "6G takes shape," *IEEE BITS the Information Theory Magazine*, vol. 4, no. 1, pp. 2–24, 2024.

[5] B. Muquet *et al.*, "Cyclic prefixing or zero padding for wireless multicarrier transmissions?" *IEEE Trans. Commun.*, v. 50, no. 12, 2002.

[6] M. Huemer, C. Hofbauer, and J. Huber, "The potential of unique words in OFDM," in *Proc. 15th International OFDM-Workshop*, Sep. 2010.

[7] A. Onic and M. Huemer, "Direct versus two-step approach for unique word generation in UW-OFDM," in *Proc. 15th International OFDM-Workshop*, Sep. 2010, pp. 145–149.

[8] C. Hofbauer *et al.*, "Coded OFDM by unique word prefix," in *Proc. IEEE International Conference on Communication Systems*, 2010.

[9] C. Hofbauer, W. H, and M. Huemer, "Pilot tone insertion and utilization in unique word OFDM," in *IEEE SPAWC*, 2020.

[10] R. Zedka *et al.*, "Unique word channel estimation for oversampled OTFS," *IEEE Transactions on Vehicular Technology*, pp. 1–17, 2026.

[11] S. A. Cheema *et al.*, "Design of space-time block coded unique word ofdm systems," in *IEEE ICASSP*, 2017, pp. 3341–3345.

[12] R. Bomfin and M. Chafii, "Unique word-based frame design for bistatic integrated sensing and communication," *IEEE Trans. Wireless Commun.*, vol. 23, no. 12, pp. 19 333–19 349, 2024.

[13] M. Huemer *et al.*, "Non-systematic complex number RS coded OFDM by unique word prefix," *IEEE Trans. Signal Process.*, vol. 60, 2012.

[14] C. Hofbauer *et al.*, "Impact of a carrier frequency offset on unique word OFDM," in *Proc. IEEE PIMRC*, 2020, pp. 1–7.

[15] H. Steendam, "Analysis of the redundant energy in UW-OFDM," *IEEE Trans. Commun.*, vol. 60, no. 6, pp. 1692–1701, 2012.

[16] ——, "On the selection of the redundant carrier positions in UW-OFDM," *IEEE Trans. Signal Process.*, vol. 61, no. 5, 2012.

[17] M. Rajabzadeh and H. Steendam, "Power spectral analysis of UW-OFDM systems," *IEEE Trans. Commun.*, vol. 66, no. 6, 2018.

[18] J. O. Smith, *Mathematics of the discrete Fourier transform (DFT): with audio applications*. Julius Smith, 2008.

[19] G. Golub and C. Loan, *Matrix Computations*, 4th ed., ser. John Hopkins Studies in Mathematical Sciences. J. Hopkins University Press, 2013.

[20] M. Rajabzadeh and H. Steendam, "Precoding for PAPR reduction in UW-OFDM," *IEEE Commun. Lett.*, vol. 25, no. 7, pp. 2390–2394, 2021.

[21] O. Lang, C. Hofbauer, and M. Huemer, "Neural network approaches for data estimation in unique word ofdm systems," *IEEE Open Journal of the Communications Society*, vol. 4, pp. 2501–2517, 2023.